

EXPERIMENTAL BENCHMARKING OF MESH SIZE AND TIME-STEP CONVERGENCE FOR A 1ST AND 2ND ORDER SWE FINITE VOLUME SCHEME

GREG COLLECUTT⁽¹⁾ & BILL SYME⁽²⁾

^(1,2) BMT WBM, Brisbane Australia,
greg.collecutt@bmtwbm.com.au

ABSTRACT

High Performance Computing (HPC) hardware is moving towards computation of accelerator devices such as GPU and Xeon Phi. These devices now enable multi-million cell hydraulic models to be solved in reasonable times, and have brought supercomputer performance to the office desktop. TUFLOW's new HPC 2D Shallow Water Equation (SWE) solver was developed with the GPU accelerator target in mind, and utilises an explicit finite volume scheme that parallelises effectively across thousands of computational cores. Along with conservation of volume, momentum, and energy, mesh size convergence is an important feature of any numerical solution scheme, and it is important for the modeller to understand how the model results change with mesh resolution. The modeller can then choose the mesh size for production runs, knowing the likely magnitude of the residual discrepancy between the production results and fully converged results. The new TUFLOW scheme is detailed, and two examples for which experimental results are available to benchmark the numerical results are presented. The first example is steady state sub-critical shallow water flow around a 90° bend, Malone et al. (2008). The second example is the United Kingdom Environment Agency (UK EA) Test 6a, UK Environment Agency (2013), in which a reservoir breaches into a confined channel with an obstruction. This model is highly transient with supercritical flow and moving hydraulic shocks. The convergence of the model results against mesh resolution and time-step is examined for these test cases, using 1st and 2nd order spatial interpolation options. Comparisons of model results against experimental data are made, and conclusions regarding "best practice" mesh resolution are drawn.

Keywords: Shallow water equations; finite volume schemes; high performance computing; model convergence; TUFLOW.

1 INTRODUCTION

Nearly every real world application for flood modelling involves estimating head losses where flows change direction. The ability of any numerical scheme to accurately compute such head losses will depend on the mathematics of the scheme, the resolution with which the geometry is modelled, and the size of the time step used for transient solutions.

In an ideal world, the key results from any model should converge asymptotically to limiting values as the model resolution is increased. However, this can be more difficult to realise in practice than at first might be thought. For one, increasing model resolution may admit new flow details to the solution that are real and expected, while for another numerical rounding error may accumulate and lead to artefact divergence in the results at very fine mesh resolutions. This may deter a modeller from performing mesh-size sensitivity studies, but there are at least three strong arguments in favour of such investigations.

Firstly, grossly changing results with mesh size may well indicate a flawed solution scheme, incorrect computer code, or poorly defined model boundary conditions (such as point sources or sinks). Mesh-size sensitivity studies should be performed if for no other reason than to build confidence in both model and software.

Secondly, mesh-size sensitivity studies may also aid in the calibration process in that some discrepancy between model results and calibration data may perhaps be understood and hence tolerated if it can be shown that the results are converging towards the calibration data as the mesh size is refined.

Thirdly, the mesh-size sensitivity study also provides a lower bound for the uncertainty in key model results, and should perhaps be added to the variations identified by other sensitivity studies such as variation in bed-friction coefficients and/or inflows.

2 TUFLOW HPC FINITE VOLUME SCHEME

The new TUFLOW HPC solver (currently branded TUFLOW GPU) evolves the 2D Shallow Water Equations (SWE) on a uniform Cartesian grid. Cell averaged depth and velocity (i.e. volume and momentum) were tracked with a finite volume scheme, and propagated forward in time using the classic fourth order Runge-Kutta method. Figure 1 illustrates the notation adopted in which the cell averaged quantities for the cell

in question are denoted with the subscript cc, the neighbouring cells are denoted n1 through to n4, the cell wall volume fluxes Φ_1 to Φ_4 . The cell width and height are Δx and Δy respectively.

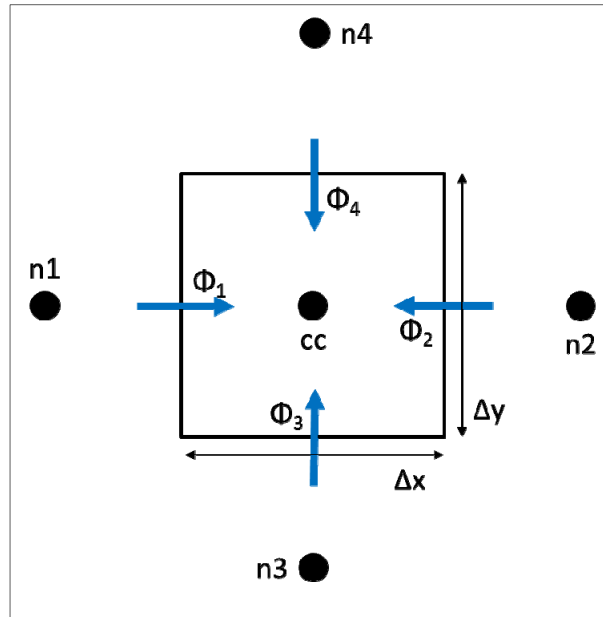


Figure 1. Finite volume notation.

The time derivative of the water depth was computed by considering conservation of volume, as expressed in Equation 1 in which A is the cell area, h is the water depth, and S_Q is any volume source or sink connected to the cell. The cell area A is considered to be time invariant. It may be modified by a 'storage reduction factor' if water displacing structures were present within the cell.

$$\frac{A\partial h}{\partial t} = \sum \Phi_i + S_Q \quad [1]$$

The volume fluxes across each face are computed using the face normal velocities, the water depth at the face, and the relevant face width. The latter may also be modified by a 'flow reduction factor' where impervious structures impede the flow. The water depth at a face was taken to be the water depth of the cell that the water was flowing from (known in computational fluid dynamics as 'upwinding'). In the case of h_1 for example, if $(u_{cc} + u_{n1}) > 0$, then h_{n1} is used, otherwise h_{cc} is used. In the case that the bed elevation of the downwind cell was higher than the bed elevation of the upwind cell, the water depth at the face was reduced by the difference in bed elevations, and limited to be non-negative.

$$\Phi_1 = \Delta y \frac{u_{cc} + u_{n1}}{2} h_1 \quad \Phi_2 = -\Delta y \frac{u_{cc} + u_{n2}}{2} h_2 \quad \Phi_3 = \Delta x \frac{v_{cc} + v_{n3}}{2} h_3 \quad \Phi_4 = -\Delta x \frac{v_{cc} + v_{n4}}{2} h_4 \quad [2]$$

In a similar manner the time derivatives of the u and v (x-dir and y-dir respectively) velocities are also computed by considering conservation of momentum in each direction, as shown in Equation 3 with the viscosity terms omitted. Here u_i , is the face interpolated u velocities, n is the Manning's bed friction coefficient, z the bed elevation, g gravity. The right most forcing term of Equation 3, forcing due to gradients in surface elevation, requires care in its discretised implementation as it can become a net source of energy within the model if incorrectly posed.

$$\frac{A\partial(hu)}{\partial t} = \sum \Phi_i u_i - Ag \frac{n^2(u^2 + v^2)^{\frac{1}{2}} u}{h^{\frac{1}{3}}} - Ag h \frac{\partial(z+h)}{\partial x} \quad [3]$$

Equation 3 requires very small time-steps to solve for u when the water depth is shallow. A more efficient implementation can be achieved by separating out the bed friction term in Equation 3, expressing it in terms of the end-of-time-step u' and v' , and solving for the end-of-time-step u' and v' implicitly using the assumption that the other forcing terms remain constant. By doing this, Equation 3 can be rearranged to Equation 4 (and similarly for v):

$$u' = \frac{u + \Delta t u_{dot}}{1 + a(u^2 + v^2)^{\frac{1}{2}}} \quad u_{dot} = \frac{1}{h} \left(\frac{\sum \Phi_i u_i}{A} - u \frac{\partial h}{\partial t} \right) - g \frac{\partial(z+h)}{\partial x} \quad a = \Delta t g \frac{n^2}{h^{\frac{4}{3}}} \quad [4]$$

u' and v' are solved iteratively together, and the effective derivatives for u and v calculated and passed to the explicit integrator.

Turbulent viscosity was modelled using the Smagorinsky formulation as shown in Equation 5, and the terms shown in Equation 6 added to the right side of Equation 3 (and similarly incorporated into Equation 4). Note that the turbulent viscosity ν_T is calculated separately at the four faces.

$$\nu_T = mA \left[\left(\frac{\partial u}{\partial x} \right)^2 + \left(\frac{\partial v}{\partial y} \right)^2 + \frac{1}{2} \left(\frac{\partial u}{\partial y} + \frac{\partial v}{\partial x} \right)^2 \right]^{\frac{1}{2}} + c \quad [5]$$

$$\Delta y \left[h_2 \nu_{T2} \frac{\partial u}{\partial x} \right]_2 - h_1 \nu_{T1} \frac{\partial u}{\partial x} \Big|_1 + \Delta x \left[h_4 \nu_{T4} \frac{\partial u}{\partial y} \right]_4 - h_3 \nu_{T3} \frac{\partial u}{\partial y} \Big|_3 \quad [6]$$

The interpolation of u and v to the cell faces can be performed either using a first order technique in which the cell average values from the upwind cell are used, or by using a second order method. The difficulty with using a pure second order method such as $u_1 = (u_{n1} + u_{cc})/2$, is that it is not total variation diminishing (TVD) and is known to be unstable. Here a hybrid technique had been adopted. To illustrate this method, consider the left face of the cell with positive flux Φ_1 . The cell average u velocity is u_{cc} , the upwind cell average u is u_{n1} , and now also consider the cell on the opposite (far) side of the upwind cell with an average u velocity of u_{11} . The hybrid technique looks at the form of the solution for u over these three cells. In the limit that the solution shows no curvature, pure second order interpolation was used, and in the limit that the solution shows reversal (i.e. u_{n1} is outside the range spanned by u_{11} and u_{cc}), then the first order scheme (upwinding) is adopted. For solutions in-between, the method blends smoothly from one to the other. Mathematically, for the case illustrated, the blend is expressed in Equation 7. In the event that flux Φ_1 is negative, u_{n2}, u_{cc}, u_{n1} are used in place of u_{11}, u_{n1}, u_{cc} respectively.

$$u_i = (1 - \xi)u_{n1} + \xi u_{cc} \quad \xi = 2x(1 - x) \quad x = \frac{u_{n1} - u_{11}}{u_{cc} - u_{11}} \quad 0 \leq x \leq 1 \quad [7]$$

The computed derivatives for h , u and v , are local in time and may be computed for each cell independently of other cells. This approach lends itself to massively parallel computation where threads were mapped to cells and each executes the same code and the order of execution is unimportant. There were a handful of data that were globally reduced (either summed or the maximum located) at each time step but efficient techniques exist for performing these reductions in a massively parallel environment.

The time evolution of the water depth and velocities was computed explicitly with the classic Runge-Kutta fourth order method. Adaptive time step size was typically employed to maintain stability of the model. The three time step control criteria were courant number N_u , celerity number N_c , and diffusion number N_d as shown in Equation 8. The time step was adjusted to maintain these at or below 1.0, 1.6, and 0.3 respectively.

$$N_u = \max \left(\frac{|u|\Delta t}{\Delta x}, \frac{|v|\Delta t}{\Delta y} \right) \quad N_c = \max \left(\frac{\sqrt{gh}\Delta t}{\Delta x}, \frac{\sqrt{gh}\Delta t}{\Delta y} \right) \quad N_d = \max \left(\frac{\nu_T \Delta t}{\Delta x^2}, \frac{\nu_T \Delta t}{\Delta y^2} \right) \quad [8]$$

2 ABRUPT ANGLED BEND TEST CASE

The TUFLOW GPU solver had been extensively tested with a wide variety of models, but there are only a few available with test data available for benchmarking. The first benchmark test considered was that of sub-critical flow around an abrupt 90 degree angled bend, as performed by Malone et. al. (2008).

Their test setup consisted of two flat bottomed flumes connected at an angle, with the downstream depth and volume flow rate able to be varied. Malone and colleagues measured the head loss attributable to the bend over a range of flow rates, water depths, bend angles, and performed a detailed analysis. The flow regimes (downstream water depth vs volume flow rate) tested are shown in Figure 2 along with a linear fit for head loss as a function of velocity head. The slope of this linear fit is the head loss factor, which represents the ratio of total energy loss around the bend to upstream kinetic energy. For the 90 degree abrupt bend, a loss factor of 1.23 was obtained.

For the majority of the tests performed, the water depths within the flumes were comparable to the flume width. This casts some doubt on the validity of modelling these tests with the SWE, but as will be shown the results agree surprisingly well.

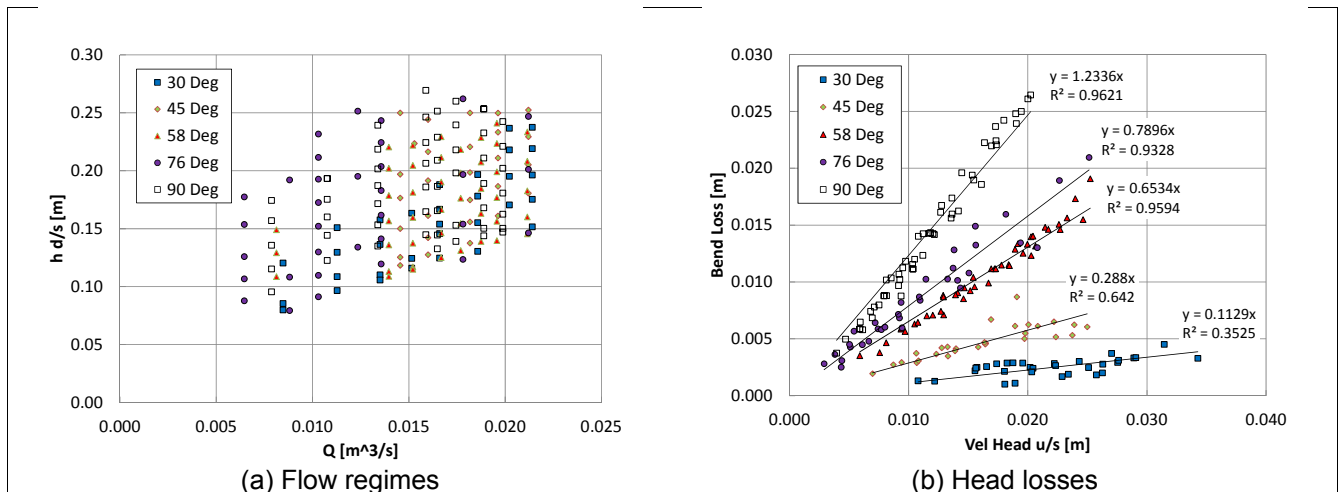


Figure 2. Abrupt angled bend test, reproduced from Malone et. al. (2008).

The first numerical study considers flow around the 90 degree abrupt bend, with flow rate of $0.008\text{m}^3/\text{s}$, and downstream water level of 0.123m . The flume width was 0.15m , and the upstream and downstream arms were 18m widths long. The bed friction (Manning's) coefficient was set to 0.01 , and both arms had a downhill gradient of 0.2% . The numerical solution was also expected to depend on mesh size, viscosity coefficients, spatial interpolation scheme, and time step. Figure 3 illustrates the flow solutions at the bend for mesh sizes ranging from 2, 4, 8 and 16 cells across the flume width resulting in mesh cell sizes less than 1 cm . Flow enters from left and exits from the bottom.

The solution was found to reach a steady state by approximately 60s from model start. Each flume arm was divided into tiles of one flume width square, and the total head in each tile was spatially and temporally averaged over 1s intervals from 60s to 120s . The total head in each tile was plotted as a function of distance from the bend, and a linear fit was derived. The head loss attributable to the bend was calculated by extrapolating the upstream and downstream linear that fits to the bend, and computing the difference.

Figure 4 plots the loss factor attributable to the bend as a function of mesh size, for the 1st and 2nd order spatial schemes and for constant viscosity values (i.e. c of Equation 5, in units m^2/s) and for proportional viscosity values (i.e. m of Equation 5, dimensionless). From these results it can be seen that both 1st and 2nd order schemes tend to over-predict the head loss, and that both 1st and 2nd order schemes with non-zero constant viscosity appear to asymptote to limiting values with decreasing cell size.

For both 1st and 2nd order schemes, the zero-viscosity case does not show convergence. A possible reason for this becomes apparent when a zero viscosity flow solution for a finer mesh size (in this case N Width = 16) was visualised, as shown in Figure 5, in which vigorous eddy structures were apparent in the flow. The introduction of some models of viscosity suppresses the intensity of these structures. Interestingly for both 1st and 2nd order schemes, non-convergence was apparent for the various proportional viscosity values trialed. A possible explanation for this behaviour is that, as the proportional viscosity term is also proportional to cell area, reducing cell size leading to zero viscosity in its limit (provided the velocity gradients within large eddies are determined by the flume width, not the mesh size).

In summary, it appears that excellent solutions were obtained with both 1st and 2nd order spatial schemes with just enough constant viscosity to prevent eddy structures in the flow. Reasonable solutions are found utilising 3 or more cells across the flume width.

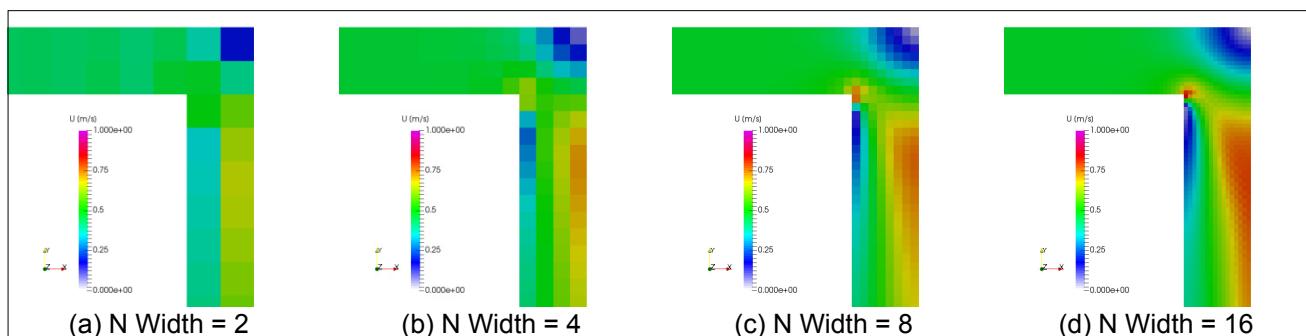


Figure 3. Flow solutions at various mesh resolutions.

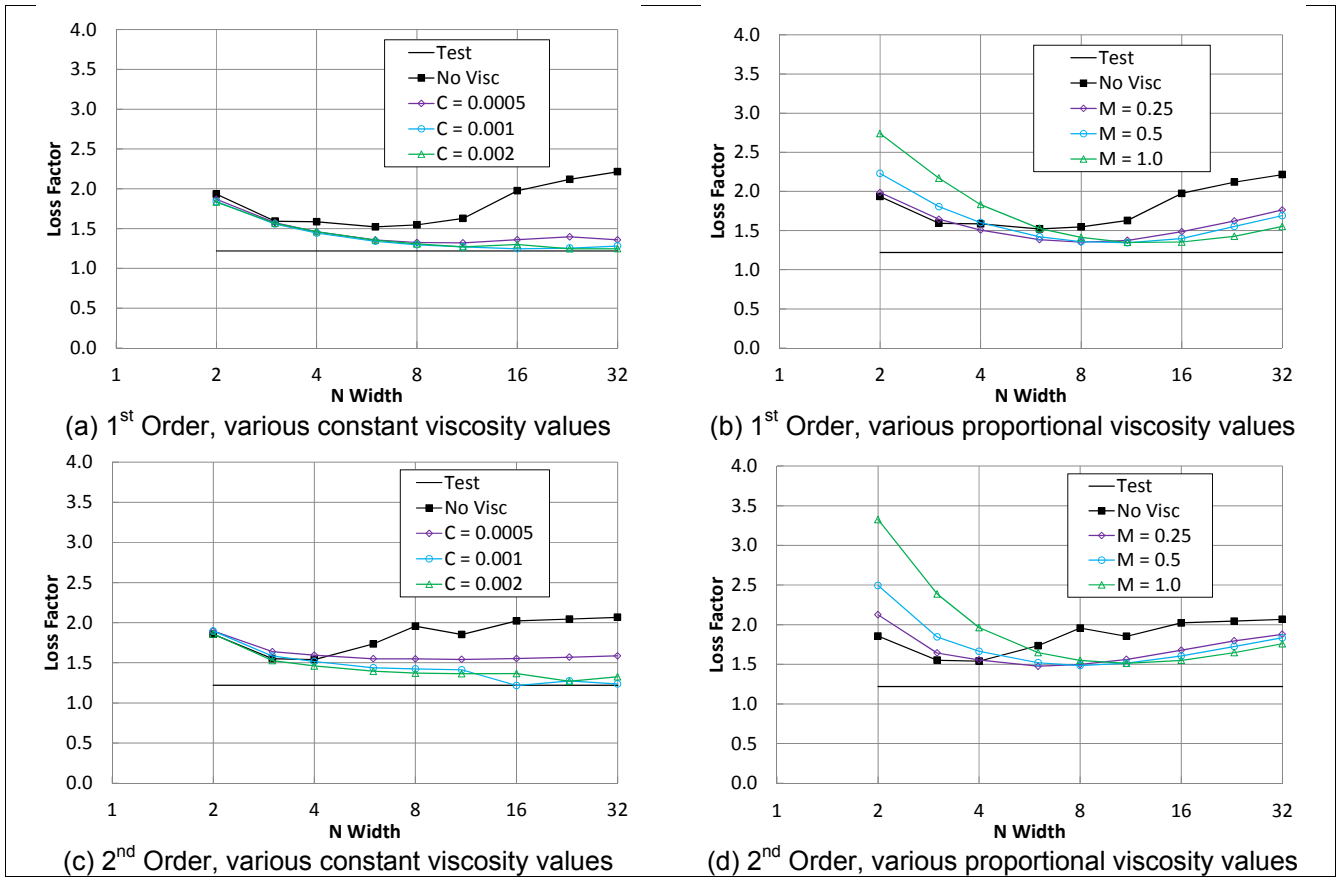


Figure 4. TUFLOW HPC Abrupt 90deg bend head loss factor.

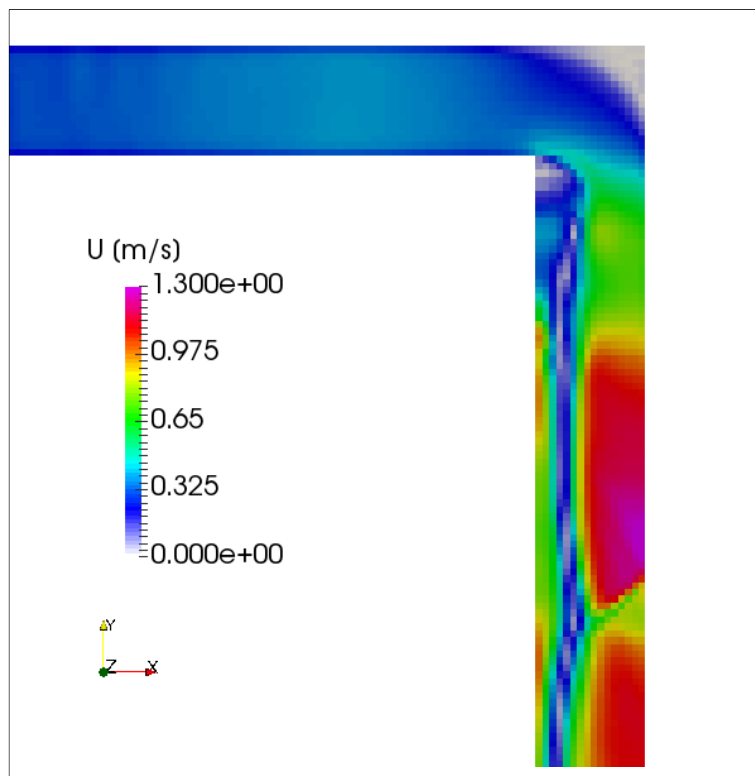


Figure 5. Eddy structures, 2nd order, zero viscosity.

Solutions for other flow rates and downstream depths were also investigated. Figure 6 shows the flow regimes considered and the resulting head losses using the 2nd order spatial scheme and a constant viscosity of $0.002\text{m}^2/\text{s}$.

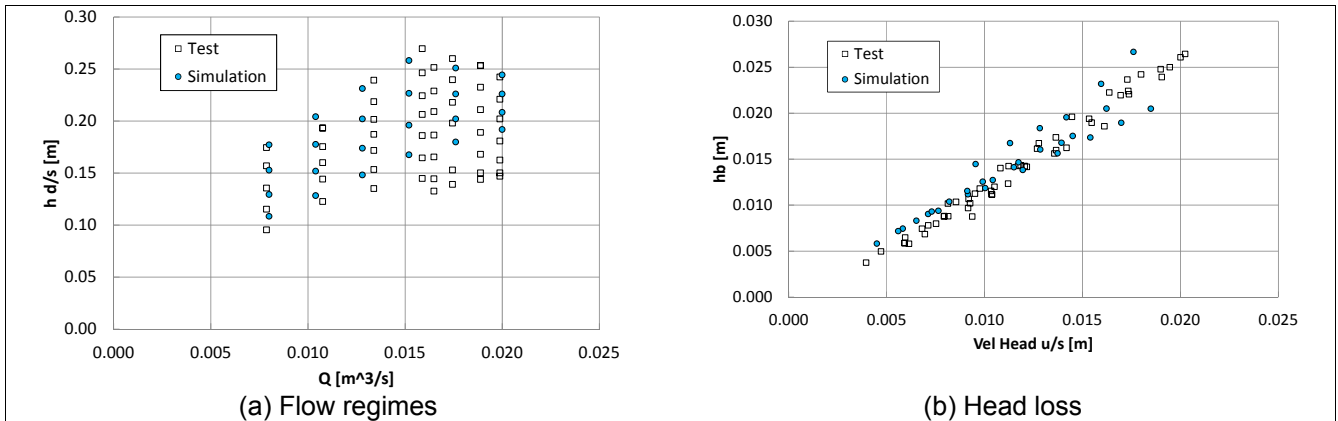


Figure 6. Abrupt 90 degree angled bend.

Malone et. al. (2008) also considered other bend angles: 30, 45, 58, and 76 degrees. Again using the same flow parameters as were used for the mesh size study, bend angles from 0 to 90 degrees in 2 degree increments were studied. The results are presented in Figure 7 using a constant viscosity of 0.002m²/s, and 8 cells across the flume width. There appears to be some scatter in the results, most likely caused by the process of discretising an angled smooth walled channel onto a Cartesian grid, but otherwise the form is promising. In general, the loss factors tend to be similar to the results obtained from the test data. One of the issues noted here is that when discretising an angled smooth walled channel onto a Cartesian grid, the apparent steps in the wall cause additional head loss in this scheme, as the flow must change direction around each step. The approach adopted within the scheme for solving this issue is to progressively modify the effective widths of the faces adjacent and perpendicular to the wall leading into and out of steps, thus allowing the flow in the cells adjacent to the wall to maintain a velocity vector parallel to the average wall line.

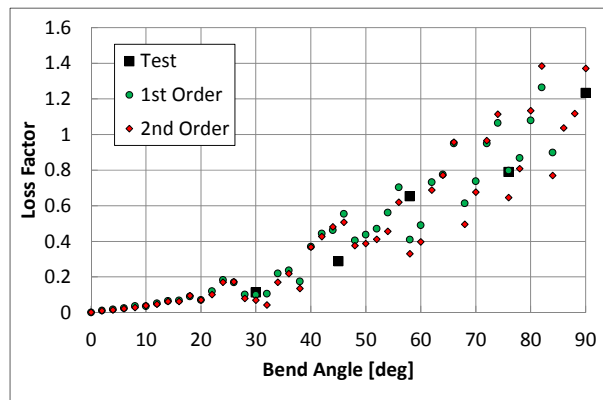


Figure 7. Head loss factor vs abrupt bend angle.

3 UK ENVIRONMENT AGENCY TEST 06A

The other test case studied for which test data were available was the dam breach model which forms part of the UK Environment Agency’s test suite, UK Environment Agency (2013). In this scaled test a reservoir was released into a long channel containing a building which obstructs the flow. This is a demanding case for comparison as the flow was highly transient and at times supercritical with moving hydraulic jumps. Figure 8 is a schematic of the test setup and a snapshot of the simulation flow velocity at time $t = 7s$ is shown in Figure 9.

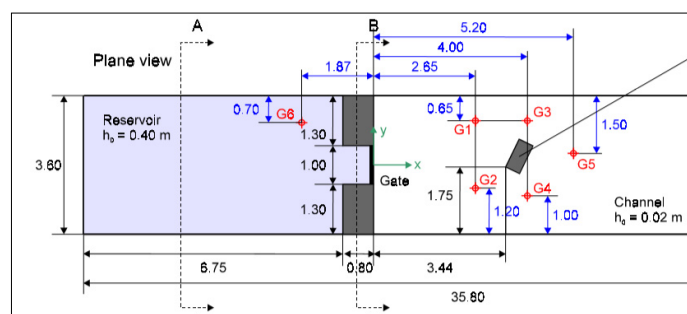


Figure 8. UK EA Test 06A, schematic.

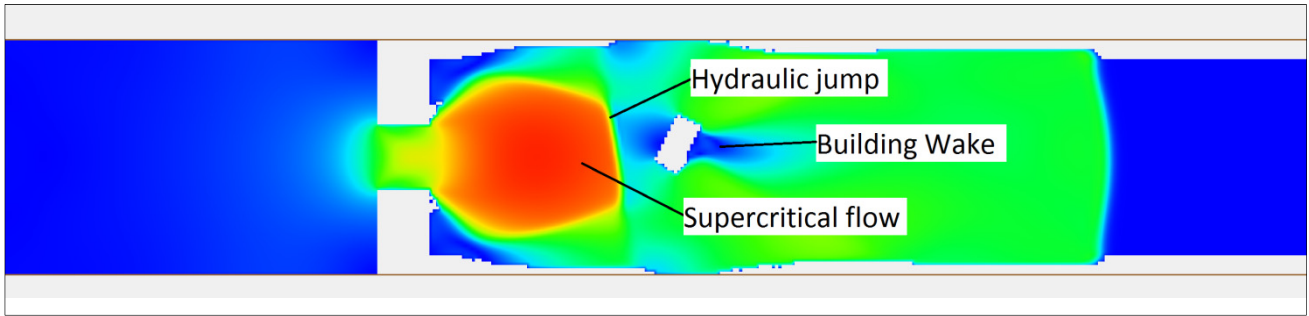


Figure 9. UK EA Test 06A, flow velocity magnitude at $t = 7s$.

More details regarding this test can be found in the UK EA test notes. The solution showed in Figure 9 was computed using the 2nd order spatial scheme, a mesh size of 0.05m, and constant viscosity of $0.05m^2/s$. Water depth and velocity were recorded at a number of gauge locations. For brevity the depth and velocity at the first three gauges are compared in Figure 10, where it can be seen that the 2nd order solution offers a better to the test results.

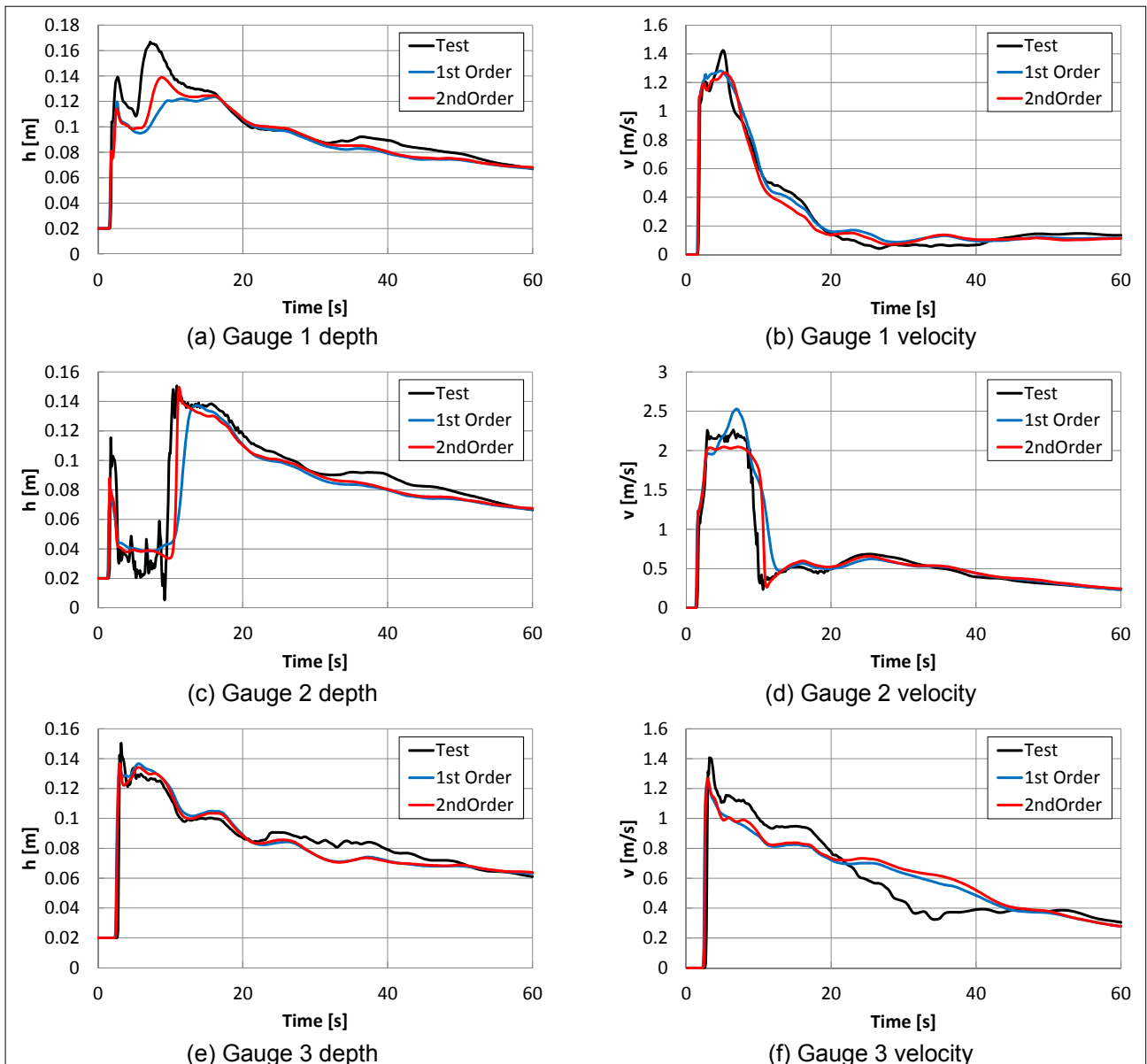


Figure 10. UK EA Test 06A, comparison of test and simulation.

Particular interest was in the results for gauge 2, in which the flow is super critical from about $t = 2s$ to $t = 10s$, and then the hydraulic jump moves upstream over the gauge at approximately $t = 10s$ and the flow becomes subcritical. The timing of this phenomenon is sensitive to the choice of viscosity coefficient and a

constant viscosity of $0.05\text{m}^2/\text{s}$ was found to be optimal. Both 1st and 2nd order schemes reproduce hydraulic jumps well. It is also worthy to note that a better fit with test data was obtained with Manning’s bed friction coefficient of 0.012 in place of the suggested 0.01 in the UK EA test notes.

Figure 11 compares the results for the depth at gauge 2 using both 1st and 2nd schemes and for the three mesh sizes 0.100m, 0.050m, and 0.025m. These results indicate that for both 1st and 2nd order schemes there was very little difference in the results between 0.050m and 0.025m cell size. The building width was 0.4m, and a mesh size of 0.05m represents 8 cells across the building.

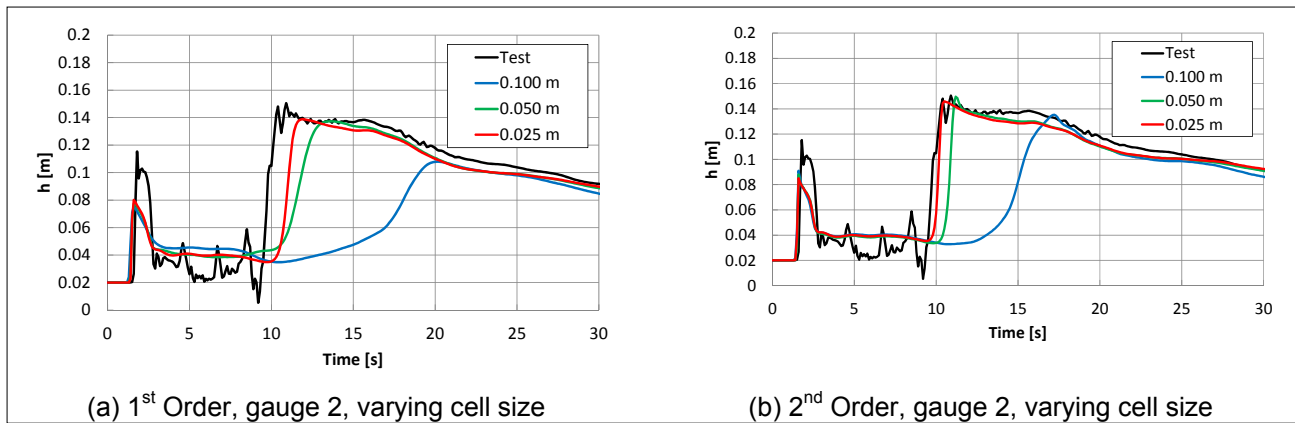


Figure 11. UK EA T06A, mesh size convergence.

As noted earlier, adaptive time-stepping was used to maintain the three control numbers N_u , N_c , N_d (Equation 8) below target limits. With many simulations, as the model evolves, the number controlling the time step may change. The scheme makes provision to run at a time step that was some fraction of the target time step, effectively causing N_u , N_c , N_d to be controlled to values that were some fraction of the default targets. The UK EA Test 06A model was re-run with a lower constant viscosity of $0.02\text{m}^2/\text{s}$, so as to cause the simulation to be courant number, controlled initially before becoming controlled diffusion number. Figure 12 represents the depth at gauge 1 using the 2nd order solver and the full target time step ($Co = 1.0$), 0.9, 0.8 and 0.7 of the target time step. Firstly note that the results for $Co = 0.7$ lie on top of the results for $Co = 0.8$ which indicates that time-step convergence has been achieved at $Co = 0.8$. Secondly note that there were small deviations from the converged results at $Co = 0.9$ and 1.0. The scheme incorporates NaN checking, and where a time step has failed the solution is wound back and the time-step repeated with a half-sized step. On successful completion of a repeated time step, the time step size was gradually increased towards the target value over successive time steps. This feature has kept both of these larger time step simulations running, even though their results in this case are of questionable quality. It is always recommended that a modeller check for time step convergence of the results, as the required time step fraction may vary with the exact particulars of the model.

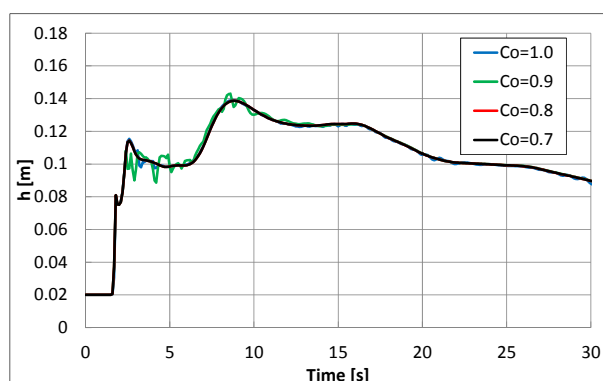


Figure 12. UK EA T06A, time step convergence, 2nd order spatial scheme (Note that results for $Co = 0.7$ overlay those for $Co = 0.8$).

4 COMPARISON WITH TUFLOW STELLING/SYME SCHEME

The abrupt 90 deg bend benchmark was solved using the established TUFLOW ADI finite difference implicit scheme as developed by Stelling and modified by Syme (1991) with the results shown in Figure 13. The ADI scheme shows some convergence with finer mesh sizes with constant only viscosity, but not with proportional only viscosity. As highlighted earlier, the proportional viscosity term becomes small in the limit of

small cell sizes and if the velocity gradients were determined by problem geometry and not mesh size. Significant interest is that with constant viscosity the Stelling/Syme scheme converges to the asymptotic limit from below, rather than from above as was the case with the new HPC scheme. This was consistent with applications of the Stelling/Syme in practice where a small amount of additional energy loss is typically required at sharp bends and flow constrictions when benchmarking and calibrating models, Syme (2001).

Of even more interest, as shown in Figure 13b, the combination of both proportional and constant viscosity terms ($M=1.00$, $C=0.005$) can generate a head-loss vs mesh size curve that is nearly flat (i.e. mesh size independent) for meshes 3 cells across the flume width and finer.

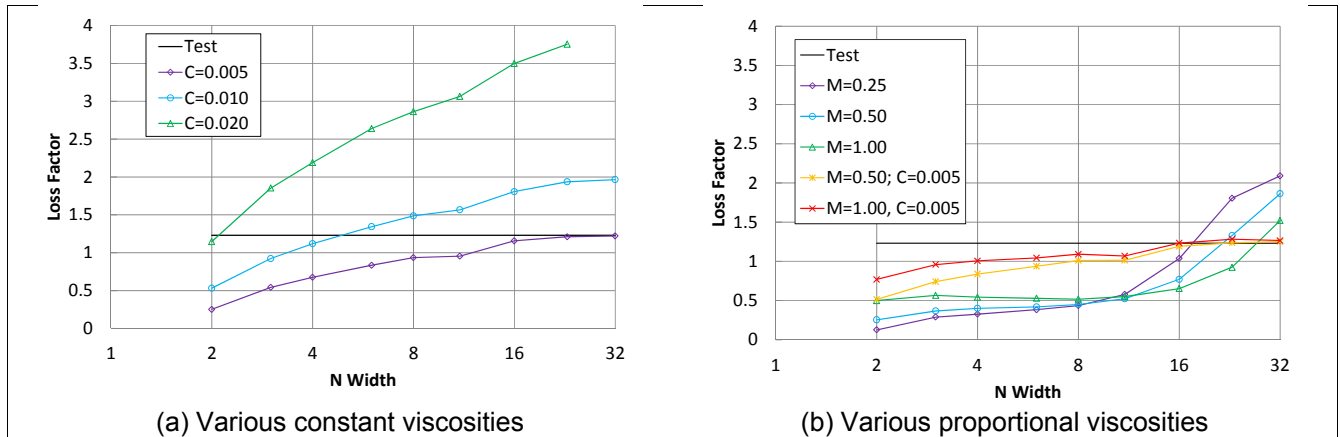


Figure 13. TUFLOW Stelling/Syme scheme, abrupt 90 deg bend head loss.

The UK EA Test 06A benchmark was also solved with the implicit Stelling/Syme scheme using the default eddy viscosity coefficients of $M=0.5$ and $C=0.05$, with the results for gauge 2 shown in Figure 14. The agreement between the two schemes is excellent, and the results for the other gauges show similar fidelity.

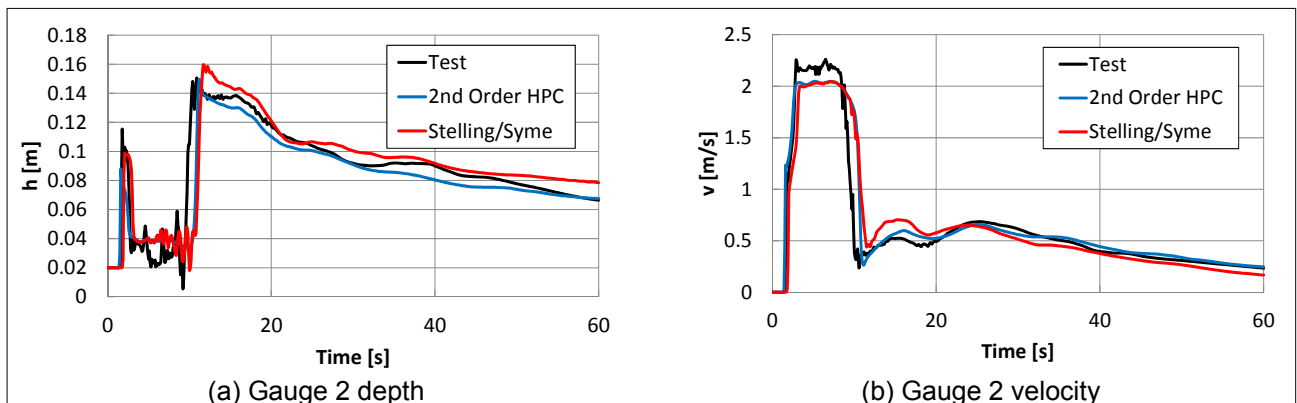


Figure 14. UK EA T06A, Gauge 2 results for 2nd order HPC and Stelling/Syme schemes, cell size 0.05m.

5 IMPLICATIONS FOR REAL WORLD APPLICATION

As shown above, the choice of Smagorinski and constant viscosity formulations has a profound effect on bend head loss estimation for the cases examined. For both the new explicit HPC scheme and the standard Stelling/Syme implicit scheme, using proportional viscosity only does not lead to mesh-size convergence and may also allow chaotic solutions to develop in the limit of very small cell sizes. For the new explicit HPC scheme, either 1st or 2nd order interpolation in combination with a small constant viscosity appears to yield excellent results. However, the optimal constant viscosity depends on the problem scale of $0.002\text{m}^2/\text{s}$ for the laboratory scale flume tests, and approximately $0.05\text{m}^2/\text{s}$ for the UK EA Test 06A. This is to be expected since the term is dimensional, and therefore its optimum value is likely to change with problem scale (and it also must be supplied in correct model units). Further research into the scale dependence of this term is needed, as the results would indicate a reducing constant viscosity coefficient with reducing problem scale.

For 90 degree bend losses, the new HPC scheme yields results that are not strongly dependent on mesh size provided the flow channels are represented by at least 3 cells across their width. In practice, it may not be possible to always have this level of mesh resolution; therefore, the impact of mesh size and choice of viscosity on key results should be investigated by the modeller prior to production runs.

It was always useful to bear in mind that a model's utility was not determined by whether it was a perfect representation of reality, but by how well it allows investigators to confidently consider as previously unseen

flow scenarios and determination of the potential impacts of material changes. Such confidence in a model's utility is derived through both calibrations against available data and sensitivity studies.

6 SUMMARY

The finite volume scheme utilised in the new TUFLOW 2D HPC solver was presented and benchmarked against test results for two distinctly different test cases.

The solver demonstrated mesh size convergence for both test cases in both 1st and 2nd order spatial interpolation schemes with a constant viscosity model. Convergence typically required 8 cells or more across feature widths, however meshes as coarse as three cells across feature widths still appear to perform well with regard to predicting head loss.

The solver demonstrated time step convergence. For the highly transient test case 'UK EA Test 06A', convergence was obtained using time steps of 0.8 of the limiting time step targets.

The solver reproduced the test results from UK EA Test 06A well including supercritical flow and hydraulic shocks/jumps.

Using only the proportional term in the Smagorinsky viscosity model, mesh size convergence is not demonstrated for either spatial scheme, possibly due to the model viscosity diminishing at smaller mesh sizes.

In the absence of viscosity, the 2nd order spatial scheme admitted eddy structures in the solution, while the 1st order solution demonstrated a dampening of eddy formation most likely due to numerical diffusion.

In terms of best practice modelling with the new HPC scheme it is recommended that

- (1) as far as practical meshes utilise three or more cells across any feature of interest;
- (2) the 2nd order spatial scheme can be selected, unless the 1st order scheme produces sufficiently similar results to the 2nd order scheme;
- (3) the overall time step control to be set to 0.8 of default targets; and
- (4) sufficient (and only sufficient) constant viscosity is used to prevent multitudes of small eddies forming in the solution.

REFERENCES

- Malone, T.R. & Parr, A.D. (2008). *Bend Losses in Rectangular Culverts*, Kansas Department of Transportation, (http://ntl.bts.gov/lib/30000/30900/30935/KU-05-5_Final_Report.pdf).
- Syme, W.J. (1991). Dynamically Linked Two-Dimensional / One-Dimensional Hydrodynamic Modelling Program for Rivers, Estuaries & Coastal Waters. *PhD Thesis*, Dept. of Civil Engineering, The University of Queensland, May 1991.
- Syme, W.J. (2001). Modelling of Bends and Hydraulic Structures in a Two-Dimensional Scheme. *The Institution of Engineers Australia Conference on Hydraulics in Civil Engineering*, Hobart.
- UK Environment Agency (2013). *Benchmarking the Latest Generation of 2D Hydraulic Modelling Packages*, Environment Agency, Horison House, Deanery Road, Bristol, BS1 9A United Kingdom, (http://evidence.environment-agency.gov.uk/FCERM/Libraries/FCERM_Project_Documents/SC120002_Benchmarking_2D_hydraulic_models_Report.sflb.ashx).